SLADE: DEVELOPMENT OF A UAV DECOY

René Heise[1], Iain K. Peddle[2], Thomas Jones[3] and Garth W. Milne[4]

[1] Department of Mechanical Engineering,
Stellenbosch University, Private Bag X1, Matieland,
7602, South Africa
e-mail: rheise@sun.ac.za

[2 3 4]Department of Electrical and Electronic Engineering,
Stellenbosch University, Private Bag X1, Matieland,
7602, South Africa
e-mail: ikpeddle@sun.ac.za
jones@sun.ac.za
milne@sun.ac.za

Key words: ducted fan, decoy, rotorcraft, control, automation

Abstract: An automated unmanned aerial vehicle demonstrator was created in order to fulfill the mission profile of a recoverable Surface Launched Aerial Decoy (SLADe). The associated quick start-up time and short flight time requirements dominated the engineering design process. Quality function deployment and basic practical considerations steered the selected vehicle configuration towards an electrically powered contra-rotating co-axial ducted fan design.

Configuration development and the vehicle design process are discussed. Where possible, the vehicle was constructed from commercial off-the-shelf components, resulting in a cost-effective and robust airframe and propulsion system. Initial vehicle flight tests were performed using a fly-by-wire stability augmentation and control system. The control system is discussed in some detail. It was designed using a derived mathematical model and simulation process. Actuation is accomplished through the use of eight control surfaces behind the rotor disks, combined with differential and collective rotor speed control.

Initial flight tests verified the vehicle's propulsion characteristics and robust airframe construction, as per the design. Stability augmentation performed well, but overall vehicle controllability is complicated by non-minimum phase longitudinal and lateral dynamics. An alternative actuation strategy, utilizing the existing actuator configuration and removing the non-minimum phase effects is suggested and will be tested. Flight automation and vehicle launch and recovery from a moving platform will receive further attention in the near future.

1 INTRODUCTION

Small Unmanned Aerial Vehicle (UAV) technologies are often optimally applied to missions where manned flight would be infeasible [1]. Such augmented roles and the associated enhanced flight capabilities currently provide the most feasible and commercially viable uses for UAVs. One such application was recently defined by the Institute for Maritime Technology (IMT), in Simon's Town, South Africa. Figure 1 illustrates this mission profile for a small decoy vehicle, carrying less than 5kg of payload (density of 1000kg/m^3). The total flight time is restricted to less than 180s and the profile includes a number of specialized flight envelope constraints.

The decoy application requires a very short time delay, only 5s, between initiation of the start-up procedure and completion of the vehicle's climb phase. At this point the UAV will be ready to perform its decoy function at 40ft Above Sea Level (ASL), traveling at less than 25m/s Air Speed (AS). After no more than 60 seconds of functional performance, the vehicle enters a recovery phase. The method of recovery should allow maximum vehicle and payload re-usability within a short time interval (as yet unspecified but probably less than one hour), and recovery should occupy a minimal amount of space on a moving platform. The vehicle guidance and control should be fully automated from start-up to completion of the recovery process, and should be accurate enough to ensure airframe yaw angle control to within 10 degrees of absolute accuracy during the mission phase. The vehicle will be operating in adverse weather conditions, including wind speeds of up to 15m/s.

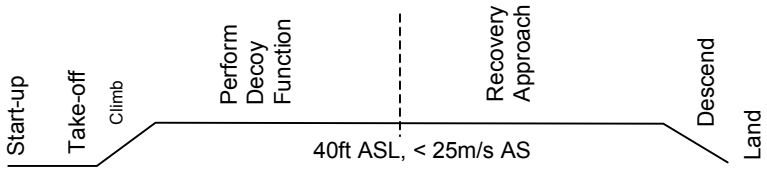

Figure 1 Mission profile of aerial decoy

As with most vehicle concepts, viability will be enhanced if a safe, reliable, low maintenance and low cost solution can be created. As such, minimal operator and ground staff training as well as minimal maintenance and ground handling requirements are desirable.

IMT tasked a four-person design team at Stellenbosch University's Faculty of Engineering to create a demonstrator UAV capable of verifying key enabling aspects of the above mission requirements. The team would focus on solving the associated high risk problems as part of this relatively low cost initial study. Mission and design requirements soon steered the team towards focusing on the development of an automated electrically powered co-axial contra-rotating ducted fan UAV.

The remainder of this document describes the engineering process followed in vehicle development as well as aspects of modeling, control, flight simulation and initial flight testing. Demonstrator development is progressing well, with an initial vehicle currently undergoing piloted fly-by-wire flight testing and evaluation. Successful flight testing will be followed by further automation and attention to launch and recovery methods.

2 CONCEPT DEFINITION

A series of design concepts were created from the mission requirements. Following a brief Quality Function Deployment (QFD) assessment, concepts were identified based on customer requirements for the four main functionalities within the UAV mission profile. The following four functionalities were identified, with their respective performance objectives:

Table 1 Functionality breakdown and objectives of the UAV

Launch concepts	Boost vehicle to 40ft altitude within 5 seconds of activation
Flight Concepts	Fly at 0 - 25m/s AS for 60 seconds, 180 seconds minimum endurance
Recovery concepts	Safely recover UAV for re-use
Motor/propulsion concepts	Provide sufficient propulsive force (~150N) for endurance of flight

Concepts were created for each functionality, with some of the concepts deliberately or knowingly conflicting with some performance requirements. Each member of the design team was then tasked to rate each concept on grounds of practical feasibility, with the top scoring concepts then being selected for further evaluation towards a final concept definition. Some concepts are only valid provided associated concerns can be successfully addressed. An example here is the use of an internal combustion engine on the UAV- there are doubts if the engine can be started reliably within the 5-second launch window. Additionally, not all the concepts for launching and recovery are compatible with the flight phase of the mission envelope. The launch and recovery concepts were initially evaluated independently from the vehicle platform configuration to form an objective opinion on the options available.

Table 2 Launch Concepts (short list)

Spring loaded launcher
Pneumatic/hydraulic Launcher
Pyrotechnic Launcher
Vehicle powered

The launch concepts were considered as a means of getting the vehicle airborne within the time limit available.

Table 3 Flight Concepts (short list)

Co-Axial Ducted Fan
Multiple Ducted Fans
Gyrocopter
Hovering Rocket

From the flight criteria of the vehicle having to maintain an AS of 0 up to 25m/s it was preconcluded that the vehicle could not be of a fixed wing configuration, unless special high-lift devices were fitted. The complexity of these configurations was deemed infeasible for the current application, and thus the concept study's short list only included rotary wing options and one rocket propelled vehicle.

Table 4 Recovery Concepts (short list)

Vertical Helicopter Landing
Conventional Arrested Landing
Harpoon to deck, with winch

Recovery options are constrained by the confined space available and will be subject to the motion of the launch/recovery platform. Additionally, it should be practically feasible for the recovery to be performed autonomously.

Table 5 Propulsion Concepts (short list)

Electric motor
Internal Combustion Engine
Jet Engine
Rocket

The prime consideration for the selection of the propulsion system is the 5 second activation-to-altitude window. This requires reliable and fast starting-up of the motor, which cannot be guaranteed when using an internal combustion engine.

3 CONCEPT EVALUATION AND SELECTION

Primary focuses for the concept selection were the flight and propulsion concepts. The difficulty of obtaining a guaranteed rapid start up time for the internal combustion and jet engine excluded these propulsion methods from further consideration. Thus only the rocket and electric motor options were studied in more detail. A direct coupling between the propulsion short list and the vehicle flight concepts exists, e.g. the electrical motor will be used with some form of rotor.

3.1 Rocket Motor

The “hovering” rocket concept uses a single rocket motor to propel the craft through the entire flight envelope, including take off and recovery. The rocket motor also sustains flight during the actual operational section of the flight envelope. The vehicle will either balance on the rocket, or if the rocket nozzle is mounted at the top of the vehicle, it would hang from the motor. Thrust vector control would be used to balance the rocket and move it away from the launch site.
An advantage of this system is that it can be launched from space efficient tubes, as the entire vehicle can be fitted into a cylindrical airframe resembling a missile. The thrust profiles of the rocket motor can be either variable or constant, with the implications of each design described below. Such "hovering" rockets are for example used by NULKA [2], where a rocket motor is pulsed, resulting in the vehicle bobbing up and down. The energy input however will remain comparable to that of a continuously variable thrust motor.

3.1.1 Variable Thrust Motor

Obtaining a suitable thrust profile from a solid or hybrid-fuelled motor in practice can be difficult. As fuel is burned off the thrust of the motor has to reduce proportionally to account for the progressively lighter vehicle, but a higher thrust setting could be required in the final stages of the flight for some recovery methods.

Designing a rocket motor that delivers a smooth and controllable thrust poses a significant technical challenge. An obvious possibility is a liquid fuelled motor since it can be designed to deliver a controllable thrust over a long time period. The complexity of such a motor will however have to be considered on a cost basis. Calculations show that for a given vehicle empty mass of 15kg specific impulse of the fuel does not significantly influence the take-off weight. Table 6 below summarizes the total take-off mass for fuel and endurance parameters of a 15kg empty mass vehicle. The figures are for sustained hovering flight only and no allowance is made for take-off and recovery.

Table 6 Total take-off mass (kg) for rocket propelled UAV

	Fuel Specific Impulse [s/kg]		
Flight time [min]	270	300	330
2	23.4	22.4	21.6
3	29.2	27.3	25.9
4	36.5	33.4	31.0

3.1.2 Constant Thrust Motor

Alternatively a rocket can be used which creates a constant thrust. This is achievable to a large extent even with solid rocket motors. The excess thrust is then dumped or pulsed by the

thrust vectoring mechanism. The rocket will have to be sufficiently large to carry the required cargo weight and the fuel mass. Table 7 lists the allowable payload mass, as a function of the specific fuel impulse used and the endurance required for a projected total vehicle mass of 15kg. For a rocket motor that produces constant thrust over the endurance period, the margin for the payload of a 15kg vehicle becomes small as the flight time increases and the specific impulse of the fuel decreases.

Table 7 Allowable payload and airframe mass (kg) for a constant 147N rocket motor

	Fuel Specific Impulse [s/kg]		
Flight time [min]	270	300	330
2	8.3	9.0	9.5
3	5.0	6.0	6.8
4	1.7	3.0	4.1

3.2 Rotor Propulsion

To obtain performance requirements of the motor(s) proposed for the UAV, simple calculations were completed based on one-dimensional momentum theory models. The calculations shown here are for an open rotor, and thus do not include the beneficial effects of a shroud. The calculations are conservative, since a carefully designed shroud can boost the rotor thrust by up to 10% under static conditions. The power the rotor absorbs is as a result of the useful thrust, so-called induced power, and the power to overcome the aerodynamic drag of turning the blades. The induced power is inversely proportional to the rotor diameter while the drag power is again proportional. Thus there is an optimum rotor diameter for which the absorbed power is a minimum.

The total weight of the vehicle is projected as 15kg, which consists of a 5kg payload and the remaining 10kg allocated for the airframe and fuel. The calculation was taken to be at standard sea level atmospheric conditions. The rotor RPM of 6000 was selected as the specified RPM of electric motors that are in question for use in the craft. Twin bladed rotors were chosen for the demonstrator for economic and logistic reasons.

The average induced velocity, v_i, required to lift the craft is calculated from momentum theory by the following equation:

$$v_i = -\frac{1}{2}v_c + \sqrt{\left(\frac{v_c}{2}\right)^2 + \frac{T}{2\rho A}} \tag{1}$$

Here A is the rotor disk area, T the rotor thrust and v_c the climb velocity of the vehicle. The rotor induced power, W, is then calculated as follows where k is a correction factor:

$$W = k\left(v_c + v_i\right)T \tag{2}$$

The power required to overcome blade drag is a function of the blade tip speed, V_t induced velocity, climb speed and blade area A_B as shown in Equation 3. The drag coefficient used here is for a NACA 0012 blade profile

$$W_D = \frac{1}{8}\rho C_D A_B \left(V_t^{\,2} + \left(V_c + v_i\right)^2\right)^{\frac{3}{2}} \tag{3}$$

For the optimum case of minimum power requirement, the blade drag power contributes 20% of the total power requirement; the variable being the rotor diameter. For the specific load case studied, the important results of the hover calculations are presented in Table 8.

Table 8 Performance parameters for the rotors

Thrust [N]	171
Number of Blades per Rotor	2
Rotor RPM	6000
Rotor Diameter [m]	0.76
Induced Velocity [m/s]	13.0
Induced Power [W]	2886
Drag Power [W]	744
Total Power per Rotor [W]	3630

4 CONCEPT SELECTION

From the final two preferred concepts, the rotor-powered option was selected, as it involved the lowest risk and complexity. The difficulty of controlling a multiple-rotor vehicle limited the configuration choices to single rotor or co-axial configuration. Though theoretically possible, the rocket-powered vehicle was deemed too complex to develop within the cost and time frame and would complicate vehicle recovery. The ducted fan is relatively easy to launch and recover, so attention was shifted from the launching and recovery concepts to the development of a flight demonstrator. It was felt that the short-listed concepts for launch and recovery could be integrated into the vehicle at a later stage. Electric propulsion was also selected at the same time, to comply with the strict start-up and launch window criteria, while allowing at least 180s of flight time.

5 DEMONSTRATOR VEHICLE DESIGN

The basic aerodynamic calculations for the rotorcraft guided the sizing of the vehicle and motor selection. From a momentum theory point of view, it is irrelevant if the actuator disk contains more than one rotor, as only a global performance is calculated. The initial performance calculation was done assuming a single rotor, to obtain the power and torque requirements for the motor. No suitable electrical motor could be found that delivers 3.6kW, and it was thus decided to use two motors instead, each with a rating of 2kW. The combined power would then also provide extra reserves to ensure a sufficiently quick climb to altitude after launch. By using the motors to drive two separate, contra-rotating rotors, the rotor torque is cancelled, thus eliminating the need for any aggressive secondary torque control measures.

The final layout of the demonstrator vehicle is a shrouded, co-axial ducted fan. The use of a shroud can increase the thrust of the rotors by up to 10% in hover. It also protects the rotor blades and handlers. The shroud was designed to give additional lift during hovering conditions, by having a wide inlet opening to utilize the low-pressure field ahead of the rotors to generate positive lift. The wide inlet opening of the shroud also provides a smooth inflow into the rotor. Additionally the shroud can be used to house cargo.

The central structure of the vehicle is used to house the motors and flight avionics, with a modular cargo bay that can be mounted either above or below the rotors. The position of the

cargo bay can be used to shift the vehicle centre of gravity for evaluation of different control strategies.
Control of the craft would be primarily through the use of flapped vanes behind the rotor disks, acting as thrust vectoring vanes. This will allow for quick, simple and accurate control inputs around all control axes. The flow straightening guide vanes also form the support struts of the motors and the additional cargo bays. The double arrangement of the guide vanes was selected for structural stiffness and the ability to mount four pairs of control vanes at the exit of the shroud.

6 DEMONSTRATOR VEHICLE CONSTRUCTION

The SLADe demonstrator, illustrated in Figure 2, was mostly constructed from materials traditionally used in the Radio Controlled (R/C) model aircraft sector. Off-the-shelf products were employed, where possible, for simplicity and to reduce costs.

The basic load carrying structure was constructed from laser-cut plywood components, constituting the two times four pairs of guide vanes and shroud cargo trays. The vehicle was constructed in an upper and lower half, the split providing maintenance access to the motors. The shroud was machined from Styrofoam and covered with an epoxy paint to protect the shroud surface. Fairings for the guide fanes were also cut from Styrofoam and covered with glass fiber/epoxy to provide stiffness. The central cargo bay/hub was constructed from glass fiber-wound tubing in which the flight control avionics were housed.

The rotor blades are standard R/C helicopter carbon fiber rotor blades with a 55mm chord, trimmed to the correct rotor diameter. The rotor blades were attached to a fixed pitch rotor hub, each driven by a 2kW brush-less DC motor.

(a)

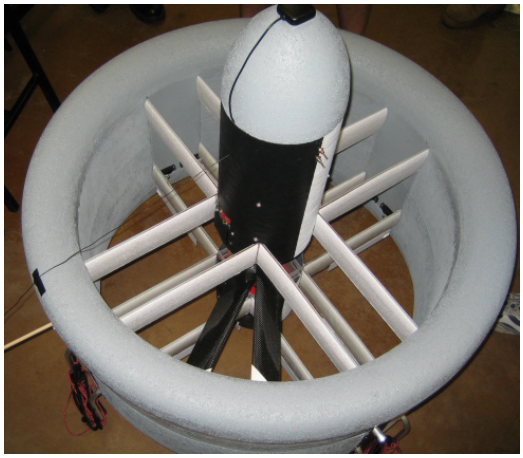

(b)

Figures 2 Two views of the completed SLADe demonstrator, showing the general layout and the double stator arrangement.

7 MODELING

An initial control system was implemented to ease pilot's workload and increase the vehicle's stability in operator controlled development tests. Simple rate-feedback loops provide artificial damping in all three axes and allow the pilot to command angular rates as opposed to angular accelerations. The following subsections discuss the details of the control system design.

7.1 Vehicle geometry and notation

Figure 3 shows a schematic diagram of the vehicle. The orientation of the body axis system with respect to the vehicle is shown. The origin O_B is located at the vehicle's centre of mass, with the Z_B-axis running along the vehicle's geometric centerline in the direction of the ducted airflow. The X_B-axis points in a predefined forward direction and the Y_B-axis completes the orthogonal, right handed axis system. The deflection angles of the eight flaps are denoted by the symbols $\delta_1 \ldots \delta_8$. A positive flap deflection is defined as one that results in further blockage of the airflow in the lightly shaded regions of Figure 3. The normalized speeds of the top and bottom rotors are denoted by the control variables δ_9 and δ_{10} respectively. The symbols r, h, d, S and A represent the radius of the duct, the height of the centre of mass above the flap's centre of pressure, the radial distance between the centre of mass and the flap's centre of pressure, the area of a flap and the cross sectional area of the duct respectively.

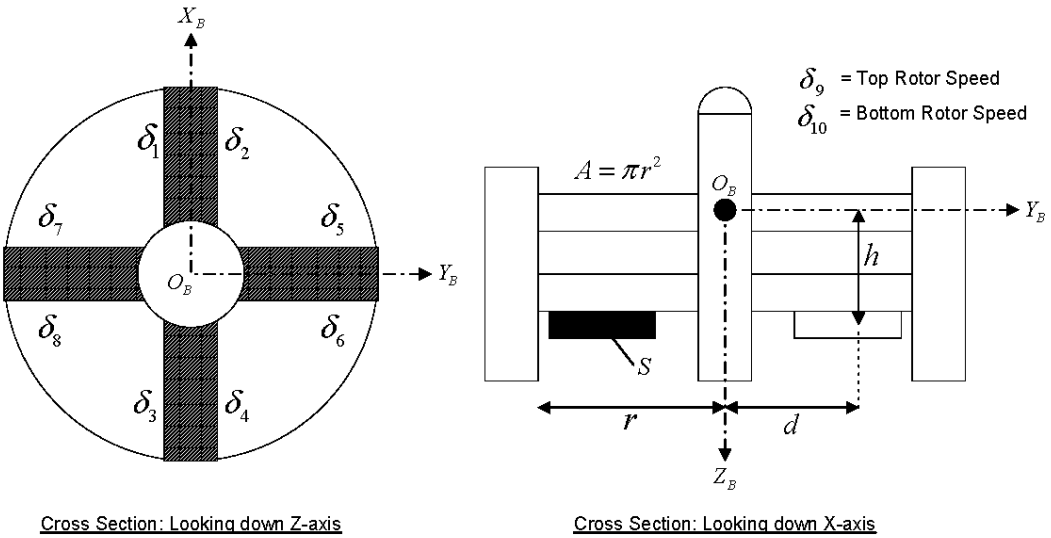

Figure 3: Schematic diagram of SLADe

7.2 Six degree of freedom equations of motion

The vehicle is modeled as a six degree of freedom rigid body. The dynamic equations describing the motion of the body axis system subject to external forces and moments are provided below [3],

$$\begin{aligned} X &= m(\dot{U} + WQ - VR) \\ Y &= m(\dot{V} + UR - WP) \\ Z &= m(\dot{W} + VP - UQ) \end{aligned} \tag{4}$$

$$\begin{aligned} L &= I_x \dot{P} + QR(I_z - I_y) \\ M &= I_y \dot{Q} + PR(I_x - I_z) \\ N &= I_z \dot{R} + PQ(I_y - I_x) \end{aligned} \tag{5}$$

$$\begin{bmatrix} \dot{\Phi} \\ \dot{\Theta} \\ \dot{\Psi} \end{bmatrix} = \begin{bmatrix} 1 & \sin\Phi\tan\Theta & \cos\Phi\tan\Theta \\ 0 & \cos\Phi & -\sin\Phi \\ 0 & \sin\Phi\sec\Theta & \cos\Phi\sec\Theta \end{bmatrix} \begin{bmatrix} P \\ Q \\ R \end{bmatrix} \tag{6}$$

$$\begin{bmatrix} \dot{N} \\ \dot{E} \\ \dot{D} \end{bmatrix} = \begin{bmatrix} C_\Psi C_\Theta & C_\Psi S_\Theta S_\Phi - S_\Psi C_\Phi & C_\Psi S_\Theta C_\Phi + S_\Psi S_\Phi \\ S_\Psi C_\Theta & S_\Psi S_\Theta S_\Phi + C_\Psi C_\Phi & S_\Psi S_\Theta C_\Phi - C_\Psi S_\Phi \\ -S_\Theta & C_\Theta S_\Phi & C_\Theta C_\Phi \end{bmatrix} \begin{bmatrix} U \\ V \\ W \end{bmatrix} \tag{7}$$

where, (X,Y,Z), (L,M,N), (U,V,W) and (P,Q,R) are the components of the force, moment, translational velocity and rotational velocity vectors coordinated in body axes respectively, (Φ,Θ,Ψ) are the Euler angles describing the attitude of the body axis system with respect to inertial space, (N,E,D) are the components of the position vector coordinated in inertial axes, m is the vehicle's mass and I_x, I_y and I_z are the moments of inertia about the respective body axes. Note that the symmetry of the vehicle about the Z_B-axis implies that the cross products of inertia are all zero.

7.3 Forces and moments

The force and moment models are simplified by only considering the vehicle at low translational velocities, where aerodynamic forces due to the translational motion of the vehicle can be ignored. Thus, only gravitational and thrust forces and moments are considered. The thrust vector is modelled as having a primary and secondary part. The primary part is due to the total thrust from the rotors and the corresponding reaction moments on the vehicle. The secondary part is due to the lift and drag (the term drag here includes the effect of flow blocking) of the flaps in the duct airflow. The forces and moments coordinated in body axes can thus be written as follows,

$$\begin{aligned} X &= qSa_L\left(\delta_5 - \delta_6 + \delta_7 - \delta_8\right) - mg\sin\Theta \\ Y &= qSa_L\left(-\delta_1 + \delta_2 - \delta_3 + \delta_4\right) + mg\cos\Theta\sin\Phi \\ Z &= qSa_D\left(|\delta_1| + |\delta_2| + |\delta_3| + |\delta_4| + |\delta_5| + |\delta_6| + |\delta_7| + |\delta_8|\right) - k_T\left(\delta_9^2 + \delta_{10}^2\right) + mg\cos\Theta\cos\Phi \\ L &= qSa_L h\left(\delta_1 - \delta_2 + \delta_3 - \delta_4\right) + qSa_D d\left(|\delta_5| + |\delta_6| - |\delta_7| - |\delta_8|\right) \\ M &= qSa_L h\left(\delta_5 - \delta_6 + \delta_7 - \delta_8\right) + qSa_D d\left(-|\delta_1| - |\delta_2| + |\delta_3| + |\delta_4|\right) \\ N &= qSa_L d\left(-\delta_1 + \delta_2 + \delta_3 - \delta_4 - \delta_5 + \delta_6 + \delta_7 - \delta_8\right) - k_M\left(\delta_9^2 - \delta_{10}^2\right) \end{aligned} \tag{8}$$

where,

$$q = k_T\left(\delta_9^2 + \delta_{10}^2\right)/A \tag{9}$$

is the dynamic pressure at the flaps, a_L is the lift coefficient of a flap per unit deflection, a_D is the drag and thrust dumping coefficient of a flap per unit deflection, k_T is the rotor thrust coefficient, k_M is the rotor moment coefficient and g is the gravitational force per unit mass.

The primary thrust forces and moments are modeled as quadratic functions of their respective rotor velocities due to their aerodynamic origin.

8 CONTROL SYSTEM DESIGN

The purpose of the control system is to ease the pilot's workload and increase the vehicle's stability for operator controlled development tests. The vehicle is over-actuated with eight flaps each capable of producing a lift and a drag force as well as two rotors each capable of producing a thrust force and a reaction moment. In order to reduce the degrees of freedom and help decouple the longitudinal, lateral, yaw and heave dynamics, the following virtual control inputs were defined.

$$\begin{aligned}
\delta_{RF} &= \left(\delta_1 - \delta_2 + \delta_3 - \delta_4\right)/4 \\
\delta_{PF} &= \left(\delta_5 - \delta_6 + \delta_7 - \delta_8\right)/4 \\
\delta_{YF} &= \left(-\delta_1 + \delta_2 + \delta_3 - \delta_4 - \delta_5 + \delta_6 + \delta_7 - \delta_8\right)/8 \\
\delta_{TR} &= \left(\delta_9 + \delta_{10}\right)/2 \\
\delta_{YR} &= \left(\delta_9 - \delta_{10}\right)/2
\end{aligned} \tag{10}$$

The subscripts of equations 1 to 5 stand for Roll-Flap, Pitch-Flap, Yaw-Flap, Thrust-Rotor and Yaw-Rotor respectively. A further five constraint equation were required in order to ensure a unique non-singular mapping between the virtual controls defined above and the original inputs.

$$\begin{aligned}
-\delta_1 + \delta_2 + \delta_3 - \delta_4 + \delta_5 - \delta_6 - \delta_7 + \delta_8 &= 0 \\
\delta_1 + \delta_2 = \delta_3 + \delta_4 = \delta_5 + \delta_6 = \delta_7 + \delta_8 &= 0
\end{aligned} \tag{11}$$

The constraints above ensure that the contribution to the yaw moment from flaps 1 to 4 is the same as that from flaps 5 to 8 and that the common mode deflection of each of the four pairs of flaps is zero.

Since all tests were limited to hover and low translational velocity flight, the vehicle model was linearized about a hover trim condition for control system design purposes. The linear state space models describing the dynamics of the vehicle about hover flight as a function of the virtual control inputs are shown below. Note that the effect of flap drag has been ignored in these models and that small letters indicate a perturbation variable.

$$\begin{bmatrix} \dot{u} \\ \dot{q} \\ \dot{\theta} \\ \dot{n} \end{bmatrix} = \begin{bmatrix} 0 & 0 & -g & 0 \\ 0 & 0 & 0 & 0 \\ 0 & 1 & 0 & 0 \\ 1 & 0 & 0 & 0 \end{bmatrix} \begin{bmatrix} u \\ q \\ \theta \\ n \end{bmatrix} + \begin{bmatrix} 4gSa_L/A \\ 4mgSha_L/I_y A \\ 0 \\ 0 \end{bmatrix} \delta_{PF} \tag{12}$$

$$\begin{bmatrix} \dot{v} \\ \dot{p} \\ \dot{\phi} \\ \dot{e} \end{bmatrix} = \begin{bmatrix} 0 & 0 & g & 0 \\ 0 & 0 & 0 & 0 \\ 0 & 1 & 0 & 0 \\ 1 & 0 & 0 & 0 \end{bmatrix} \begin{bmatrix} v \\ p \\ \phi \\ e \end{bmatrix} + \begin{bmatrix} -4gSa_L/A \\ 4mgSha_L/I_x A \\ 0 \\ 0 \end{bmatrix} \delta_{RF} \tag{13}$$

$$\begin{bmatrix} \dot{r} \\ \dot{\psi} \end{bmatrix} = \begin{bmatrix} 0 & 0 \\ 1 & 0 \end{bmatrix} \begin{bmatrix} r \\ \psi \end{bmatrix} + \begin{bmatrix} 8mgSa_L d/I_z A & -k_M\sqrt{8mg/k_T}/I_z \\ 0 & 0 \end{bmatrix} \begin{bmatrix} \delta_{YF} \\ \delta_{YR} \end{bmatrix} \tag{14}$$

$$\begin{bmatrix} \dot{w} \\ \dot{d} \end{bmatrix} = \begin{bmatrix} 0 & 0 \\ 1 & 0 \end{bmatrix} \begin{bmatrix} w \\ d \end{bmatrix} + \begin{bmatrix} -\sqrt{8k_T g/m} \\ 0 \end{bmatrix} \delta_{TR} \tag{15}$$

Due to the symmetry of the vehicle, the roll and pitch dynamics are of exactly the same form. Roll and pitch rate feedback was implemented using the following control laws,

$$\begin{aligned} \delta_{RF} &= K_p \left(p_c - p \right) \\ \delta_{PF} &= K_q \left(q_c - q \right) \end{aligned} \tag{16}$$

where, p_c and q_c are the pilot's roll and pitch rate commands and K_p and K_q are the feedback gains selected to provide the desired dynamic response. The yaw dynamics constitute a multi-input system. The control system uses the high frequency flap actuators to provide yaw damping and ease the pilot workload during flight. However, countering low frequency yaw moments using the flaps is not ideal since it increases the drag in the duct and decreases the available dynamic range of the flaps. Thus, a low frequency yaw moment controller is also implemented using the differential rotor speed control input, thus relieving the flaps from this duty. The time constant of this controller was selected as 5s which is slow enough to allow the rotor speed dynamics to be ignored. The controller implemented is shown below and in block diagram form in Figure 4.

$$\begin{aligned} \delta' &= K_r \left(r_c - r \right) \\ \dot{x} &= -x/\tau + \delta'/\tau \\ \delta_{YF} &= \delta' - x \\ \delta_{YR} &= K_a x \end{aligned} \tag{17}$$

Here, r_c is the pilot's yaw rate command, K_r is the yaw rate damper feedback gain selected to yield the desired dynamic response, τ the flap washout time constant, x the internal low pass filter state and,

$$K_a = -Sa_L d\sqrt{8mgk_T} \,/ k_M A \tag{18}$$

the gain that ensures that δ_{YF} and δ_{YR} produce the same yaw moment. The sensitivity of the closed loop system (i.e. control system and pilot in the loop) to the gain K_a will be zero in the steady state due to a human pilot's natural integral control of error signals. Furthermore, the washout response between the flaps and the differential rotor speed is slow enough to ensure that the pilot will be capable of maintaining a stable closed loop system.

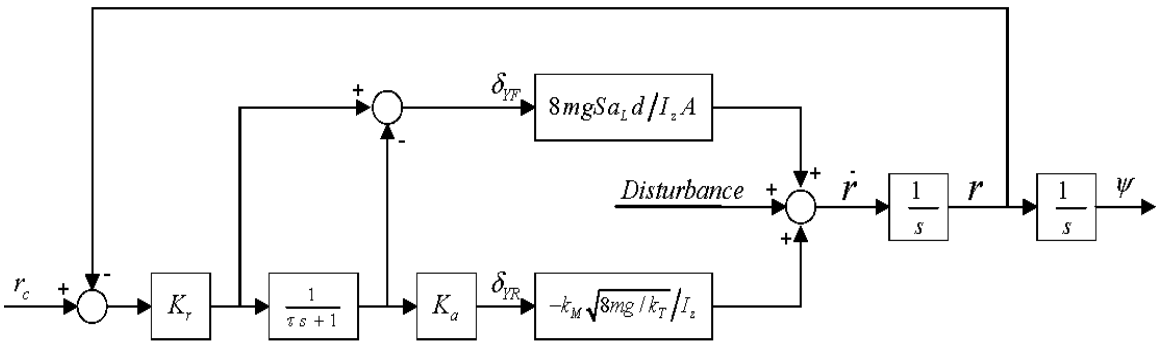

Figure 4: Yaw rate control system

A controller similar to that of the yaw rate controller could have been used to regulate the altitude i.e. the flaps could be used to provide high frequency thrust dumping while changing the total thrust from the rotors could provide the low frequency actuation. However, this control strategy was not adopted for the initial piloted flight tests as the dynamic response of the electric motors was deemed acceptably fast for good height control.

9 SIMULATION

Simulation results using the parameters given in Table 9 for the vehicle are shown in Figure 5. The response to a 15 deg/s step command in roll/pitch is shown in the left column of Figure 5. The right column of Figure 5 illustrates the working of the yaw control system. At time zero, a yaw disturbance torque of 0.5 Nm is applied to the system. Note how the flaps ensure a fast dynamic response in rejecting the disturbance torque. After the transient period, the flaps slowly return to their neutral positions while the differential motor speed is adjusted to leave the yaw output unchanged. After 10s, the pilot provides a command input to negate the steady state yaw rate and similar results are seen in the control inputs.

Table 9: Numerical values of symbols for SLADe

Symbol	Value	Unit	Symbol	Value	Unit
d	0.3	m	I_x	0.5	kg m^2
h	0.3	m	I_y	0.5	kg m^2
r	0.4	m	I_z	0.5	kg m^2
S	0.008	m^2	a_L	4	ND
A	0.5	m^2	k_T	100	kgm/s^2
m	12	kg	k_M	3	kgm^2/s^2

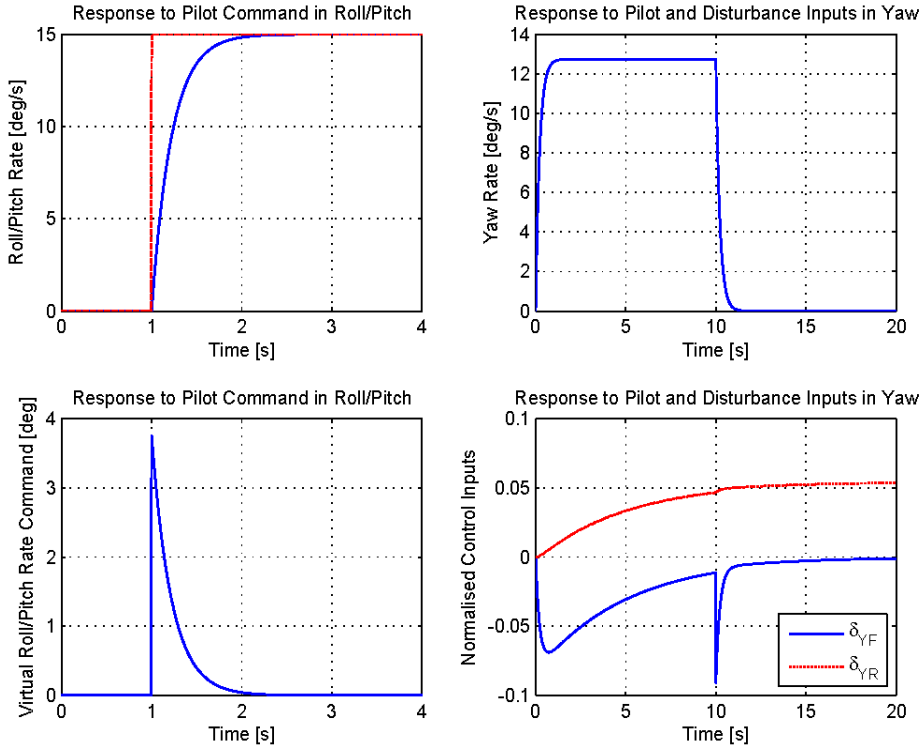

Figure 5: SLADe Simulation results

10 FLIGHT TEST RESULTS

The control system was implemented onboard the vehicle using the in-house developed Electronic Systems Laboratory (ESL) Advanced UAV Avionics stack, based on a Linux powered PC-104 Plus PIII 300MHz equivalent CPU with CAN-bus enabled sensor technology [4,5].

From pilot feedback, it was concluded that the stability augmentation system worked well in practice. However, the major difficulty in controlling the vehicle stemmed from the non-minimum phase nature of the longitudinal and lateral dynamics. Since these two sets of dynamics are of exactly the same form (see Equations 12 and 13), only the lateral dynamics will be discussed.

The transfer function from the virtual roll actuator to lateral velocity has a non-minimum phase zero at,

$$z = \sqrt{gh\,m/I_x} = \sqrt{gh}/r_G \tag{19}$$

where r_G is the vehicle's radius of gyration. This zero is due to the nature of the virtual roll actuator. In order to increase lateral velocity, a positive roll moment is required to rotate the thrust vector such that the desired lateral acceleration is produced. However, to produce a positive roll moment requires flaps 1 to 4 to be deflected in such a way that a negative lateral force is produced. Until this force is overcome by the rotated thrust force, the vehicle will begin the move in the 'wrong' direction; a defining characteristic of non-minimum phase systems.

From this argument and from Equation 19, it is clear that the relationship between the vehicle's mass and its moment of inertia about the axis in question is of importance in determining the location of the non-minimum phase zero. The location of the zero is important because it places an upper bound on the bandwidth achievable by any control system [6] with finite actuation power. This fact, together with the obvious convenience, promoted placing the avionics and battery packs in the centre of the vehicle as opposed to in the shroud. With this configuration the vehicle had an estimated radius of gyration of approximately 0.2 m (refer to Table 9) and thus a non-minimum phase zero at approximately 1.3 Hz. This frequency was deemed high enough for position and velocity control.

However, in spite of these efforts, it was found that the pilot struggled to control the vehicle due to its non-minimum phase nature. The difficulties are further exacerbated when the vehicle is flown just above the ground where the clearance is too little for the vehicle to roll through the necessary angle to produce the desired lateral acceleration. In these conditions the adverse acceleration dominates, which in effect reverses the pilot's roll and pitch controls!

To circumvent this problem, the method of roll and pitch actuation will be changed for all future research. Instead of deflecting the flow to produce a lateral lifting force which in turn creates the desired moment, a thrust dumping method (with larger flaps) will be used. Here, the flaps are used to close off the duct in certain quadrants and thus reduce the net thrust there. This strategy will completely eliminate the non-minimum phase nature of the system.

11 CONCLUSIONS

The design of an electrically powered contra-rotating co-axial ducted fan is described, in solution to the given mission profile. Various alternative vehicle options were evaluated, but quick start-up time and short flight time requirements dominated the engineering design process. The ducted fan configuration poses the simplest known solution to these requirements.

Initial fly-by-wire flight tests verified the vehicle's propulsion characteristics and robust airframe construction, as per the design. Stability augmentation performed well, but overall vehicle controllability is complicated by non-minimum phase longitudinal and lateral dynamics. An alternative actuation strategy, utilizing the existing actuator configuration and removing the non-minimum phase effects was suggested and will be used for future flight tests.

Flight automation and vehicle launch and recovery from a moving platform will receive further attention in the near future.

12 ACKNOWLEDGEMENTS

The above research and development was completed at the Faculty of Engineering, Stellenbosch University, under a research grant from the Institute for Maritime Technology (http://www.imt.co.za) managed by Lleon Downes and Danie Bence. The majority of the work was executed in the Electronic Systems Laboratory (htp://esl.ee.sun.ac.za), and forms part of a wider autonomous flight research activity.

13 REFERENCES

[1] Lester Ingham, Thomas Jones and Anton Maneschijn, "Certification of Unmanned Aerial Vehicles in South African Airspace", R&D Journal, Volume 22, Number 1, SAIMechE, March 2006

[2] John Liang, "Navy's Aegis Destroyers Will Be First To Get New Anti-Ship Missile Decoy", Inside Missile Defense, Sept 1997, pp 1-16

[3] John H. Blakelock, *"Automatic Control of Aircraft and Missiles, Second Edition"*, John Wiley and Sons, New York, 1991

[4] Stephanus Groenewald, "Development of a Rotary-Wing Test Bed for Autonomous Flight", Masters Degree Thesis, Stellenbosch University, February 2006

[5] Jacob Venter, "Development of an Experimental Tilt-Wing VTOL Unmanned Aerial Vehicle", Masters Degree Thesis, Stellenbosch University, February 2006

[6] Graham C. Goodwin, Stefan F. Graebe, Mario E. Salgado, *"Control System Design"*, Prentice Hall, Upper Saddle River, NJ, USA, 2001